Wideband laser-interferometer graviational-radiation experiment

Robert L. Forward
Hughes Research Laboratories, Malibu, California 90265
(Received 12 September 1977)

A wideband laser-interferometer gravitational-radiation antenna was constructed and used to search for gravitational radiation in the frequency band from 1 to 20 kHz. The antenna consisted of a Michelson interferometer with the beamsplitter and retroreflectors attached to masses on soft suspensions that allowed essentially free motion above the suspension frequencies. The strains in the gravitational radiation produce a differential path length change in the two arms of the interferometer which is detected by a pair of balanced photodetectors. The interferometer used a folded-path configuration with an effective length of 8.5 m. The sensitivity of the interferometer was calibrated with signals from a piezoelectric displacement transducer. The strain noise in a 1-Hz bandwidth was less than 0.3 fm/m from 1 to 3 kHz, and less than 0.1 fm/m above 3 kHz, where it was essentially photon-noise limited. (For comparison, the kT strain noise in a room-temperature, 2-m long, 1000-kg, elastic solid bar antenna is 0.14 fm/m.) The laser interferometer was operated as a detector for gravitational radiation for 150 h during the nights and weekends from the period 4 October through 3 December 1972. During the same period, bar antennas were operated by the Maryland, Glasgow, and Frascati groups, with 18 events reported by the Frascati group in their single bar, 22 single-bar events and no coincidences reported by the Glasgow group in their two bars, and 28 coincidences reported by the Maryland group between the Argonne bar and the Maryland bar and/or disk antennas. The various bar antenna systems were quite different but in general were sensitive to gravitational-radiation strain spectral components with an amplitude of the order of 0.1 fm/m in a narrow band of frequencies about the resonant frequency of the bar. The wideband interferometer data was analyzed by ear, with the detection sensitivity estimated to be of the order of 1–10 fm/m (depending upon the signature of the signal) for the total of the gravitational-radiation strain spectral components in the band from 1–20 kHz. No significant correlations between the Malibu interferometer output and any of the bar events or coincidences were observed.

I. WIDEBAND INTERFEROMETER ANTENNA

The wideband laser-interferometer gravitational-radiation antenna consists of a laser-excited Michelson interferometer with the beamsplitter and reflectors attached to kilogram-sized masses on soft suspensions that allow essentially free motion above the suspension frequencies. As shown in Fig. 1, when the direction of gravitational radiation is along one of the interferometer arms, that arm does not experience any differential motion between the beamsplitter and retroreflector, and thus acts as a reference arm for the interferometer. The strains produced by the gravitational radiation (of proper polarization) then act on the other arm of the interferometer, causing a differential ac motion of the beamsplitter and retroreflector at the frequency of the gravitational radiation.[1,2] When the direction of the gravitational radiation is at right angles to the plane of the interferometer, one arm will decrease in length and the other will increase, resulting in a doubling of the signal.

A. Coupling of radiation to antenna

Gravitational radiation couples to the laser-interferometer antenna by causing relative motion between the beamsplitter and mirrors in the interferometer. The strains and relative motions induced by the gravitational radiation are readily derived from the weak-field approximation to the Einstein field equations,

$$R_{\alpha\beta} - \tfrac{1}{2} g_{\alpha\beta} R = \frac{8\pi G}{c^4} T_{\alpha\beta} \ . \tag{1}$$

The gravitational-radiation field is assumed to be a weak perturbation on the metric $g_{\alpha\beta} = \eta_{\alpha\beta} + h_{\alpha\beta}$, that propagates as a tensor wave:

$$\frac{\partial^2 h_{\alpha\beta}}{\partial x_\alpha^{\,2}} - \frac{1}{c^2} \frac{\partial h_{\alpha\beta}}{\partial t^2} = 0 \ . \tag{2}$$

The general form of a gravitational wave propagating in the z direction will have the character[3]

$$h_{\alpha\beta} = (h_t t_{\alpha\beta} + h_s s_{\alpha\beta}) e^{-i(\omega t - kz)} \ , \tag{3}$$

where h_t and h_s are the scalar amplitudes of the two states of polarization of the wave. For linearly polarized radiation one state of polarization is the tension-compression polarization represented by

$$t_{\alpha\beta} = \begin{bmatrix} 0 & 0 & 0 & 0 \\ 0 & 1 & 0 & 0 \\ 0 & 0 & -1 & 0 \\ 0 & 0 & 0 & 0 \end{bmatrix} \tag{4}$$

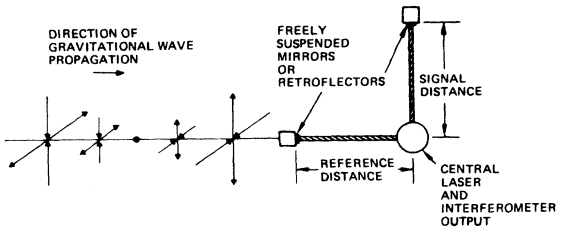

FIG. 1. Wideband laser-interferometer antenna.

or $h_{11} = -h_{22}$, which consists of a tension along the x axis and a compression along the y axis [see Fig. 2(a)].

The other state of polarization is the shear polarization represented by

$$s_{\alpha\beta} = \begin{bmatrix} 0 & 0 & 0 & 0 \\ 0 & 0 & 1 & 0 \\ 0 & 1 & 0 & 0 \\ 0 & 0 & 0 & 0 \end{bmatrix} \tag{5}$$

or $h_{12} = h_{21}$, which consists of shear forces along the bisectors of the x and y axes [see Fig. 2(b)]. From inspection it is easily seen that the two polarizations are orthogonal since $s_{\alpha\beta} t^{\alpha\beta} = 0$ and that the shear polarization $s_{\alpha\beta}$ is just the tension polarization rotated through 45° (demonstrating the spin-2 characteristics of the radiation).

If desired, the flux of this gravitational radiation in power per unit area can be obtained from the relation[4]

$$I = \frac{c^3}{16\pi G}\left[\dot{h}_{12}^{\,2} + \tfrac{1}{4}(\dot{h}_{11} - \dot{h}_{22})^2\right] . \tag{6}$$

Each arm of the interferometer consists of a pair of freely suspended masses holding a beam-splitter or a retroreflector and separated by a distance $\xi^\beta = l^\beta + \xi^\beta(t)$, where l^β is the nominal separation distance of the masses without excitation, and $\xi^\beta(t)$ is the time-varying portion of the displacement caused by the radiation.

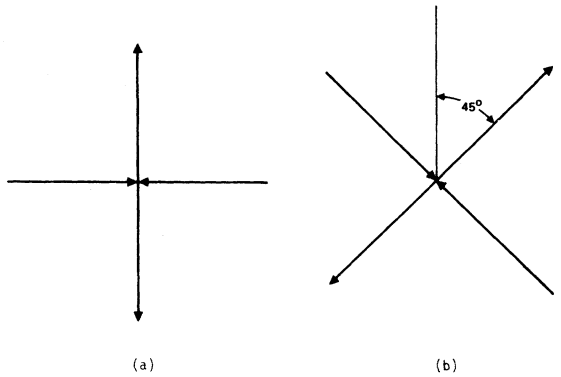

FIG. 2. The two states of polarization of tensor gravitational radiation.

The gravitational radiation interacts with the pair of masses through the equation of geodesic deviation for small, nonrelativistic motions as follows:

$$\frac{d^2\xi^\beta}{dt^2} = -c^2 R^\beta{}_{0\alpha 0}\xi^\alpha \approx -c^2 R^\beta{}_{0\alpha 0} l^\alpha . \tag{7}$$

If the detecting masses are entirely free, then the equations simplify to give the relative displacement ξ^β between the masses in terms of the gravitational-field strength,

$$\ddot{\xi}^\beta = -c^2 R^\beta{}_{0\alpha 0} l^\alpha = \tfrac{1}{2}\ddot{h}^\beta{}_\alpha l^\alpha . \tag{8}$$

The equivalent strain $\epsilon^\beta{}_\alpha = \xi^\beta / l^\alpha$ over the distance l^α is then given by

$$\ddot{\epsilon}^\beta{}_\alpha = -c^2 R^\beta{}_{0\alpha 0} = \tfrac{1}{2}\ddot{h}^\beta{}_\alpha , \tag{9}$$

which shows that the strain is a direct measure of the gravitational-field strength.

The Michelson interferometer used as the antenna consists of two orthogonal arms of the same nominal length l. The interferometer produces a change in output when there is a difference in the two path lengths. For an antenna with one arm along the x axis and the other along the y axis, the output is

$$\xi^1 - \xi^2 = \tfrac{1}{2}(h^1{}_1 l^1 - h^2{}_2 l^2) \tag{10}$$

or

$$\Delta\xi = \tfrac{1}{2}(h_{11} - h_{22})l = lh , \tag{11}$$

where $h_{\alpha\beta}$ is measured in the coordinate system of the antenna. This scalar output can be obtained by assuming a tensor format for the combined response of the two arms of the antenna

$$A^{\alpha\beta} = \begin{bmatrix} 0 & 0 & 0 & 0 \\ 0 & 1 & 0 & 0 \\ 0 & 0 & -1 & 0 \\ 0 & 0 & 0 & 0 \end{bmatrix} l , \tag{12}$$

and carrying out the operation

$$\Delta\xi = \tfrac{1}{2} h_{\alpha\beta} A^{\alpha\beta} . \tag{13}$$

B. Detection-sensitivity pattern

The detection-sensitivity pattern of the laser-interferometer antenna for the gravitational radiation of different polarizations coming from different directions is a complex one.

In Fig. 3 we assume that the laser-interferometer antenna lies in the x-y plane with one arm along the x axis and the other along the y

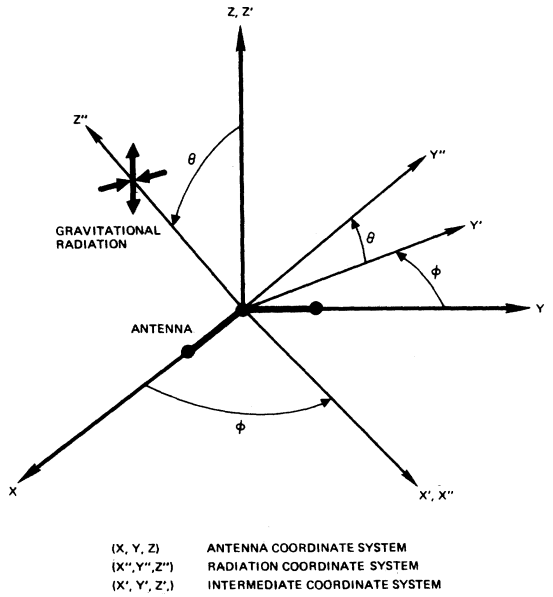

FIG. 3. Coordinates for calculation of interaction of antenna with radiation.

axis, while the gravitational radiation is arriving from an arbitrary direction (θ, ϕ) with an arbitrary polarization. In the coordinate system (x'', y'', z'') of the gravitational radiation, we can separate the radiation into its two linear polarizations $t_{\alpha\beta}$, with the tension lying in the x-y plane of the antenna, and $s_{\alpha\beta}$ at 45° to it.

To convert the two tensor polarizations from the radiation-coordinate system to the antenna-coordinate system, we use the general form of the rotation matrix[5] with $\psi = 0$:

$$R^{\alpha}_{\beta} = \begin{bmatrix} 1 & 0 & 0 & 0 \\ 0 & \cos\phi & \sin\phi & 0 \\ 0 & -\cos\theta\sin\phi & \cos\theta\cos\phi & \sin\theta \\ 0 & \sin\theta\sin\phi & -\sin\theta\cos\phi & \cos\theta \end{bmatrix} . \tag{14}$$

Plane-polarized radiation propagating along the z'' direction and polarized along the x''-y'' direction

$$h''_{\alpha\beta} = h_t t''_{\alpha\beta} = \begin{bmatrix} 0 & 0 & 0 & 0 \\ 0 & 1 & 0 & 0 \\ 0 & 0 & -1 & 0 \\ 0 & 0 & 0 & 0 \end{bmatrix} h_t , \tag{15}$$

is then converted by the rotation matrix into the antenna-coordinate system by the operations

$$t_{\alpha\beta} = R^{-1}{}_{\alpha}{}^{\gamma} t''_{\gamma\delta} R^{\delta}{}_{\beta} , \tag{16}$$

or

$$t_{\alpha\beta} = \begin{bmatrix} 0 & 0 & 0 & 0 \\ 0 & \cos^2\phi - \cos^2\theta\sin^2\phi & (1+\cos^2\theta)\sin\phi\cos\phi & \sin\theta\cos\theta\sin\phi \\ 0 & (1+\cos^2\theta)\sin\phi\cos\phi & \sin^2\phi - \cos^2\theta\cos^2\phi & -\sin\theta\cos\theta\cos\phi \\ 0 & \sin\theta\cos\theta\sin\phi & -\sin\theta\cos\theta\cos\phi & -\sin^2\theta \end{bmatrix} . \tag{17}$$

The antenna response to this polarization is

$$\Delta\xi = \tfrac{1}{2} h_{\alpha\beta} A^{\alpha\beta} = \tfrac{1}{2} h_t t_{\alpha\beta} A^{\alpha\beta}$$
$$= \tfrac{1}{2} h_t l (1+\cos^2\theta)\cos 2\phi . \tag{18}$$

The shape of the antenna-response pattern in the azimuthal and polar directions are given in Fig. 4.

Plane-polarized radiation propagating along the z'' direction and polarized in the shear direction to the x''-y'' axes,

$$h''_{\alpha\beta} = h_s s''_{\alpha\beta} = \begin{bmatrix} 0 & 0 & 0 & 0 \\ 0 & 0 & 1 & 0 \\ 0 & 1 & 0 & 0 \\ 0 & 0 & 0 & 0 \end{bmatrix} h_s , \tag{19}$$

is converted by the rotation matrix into the antenna-coordinate system by

$$s_{\alpha\beta} = R^{-1}{}_{\alpha}{}^{\gamma} s''_{\gamma\delta} R^{\delta}{}_{\beta} \tag{20}$$

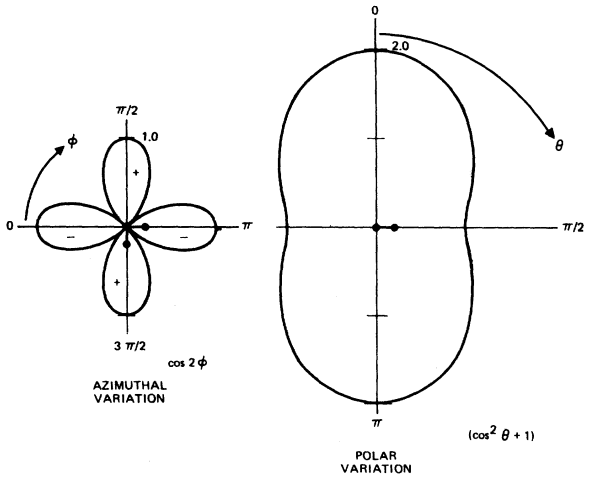

FIG. 4. Detection sensitivity pattern for linearly polarized gravitational radiation with one direction of polarization in plane of the antenna.

or

$$s_{\alpha\beta} = \begin{bmatrix} 0 & 0 & 0 & 0 \\ 0 & -\sin 2\phi \cos\theta & \cos 2\phi \cos\theta & \cos\phi \sin\theta \\ 0 & \cos 2\phi \cos\theta & \sin 2\phi \cos\theta & \sin\phi \sin\theta \\ 0 & \cos\phi \sin\theta & \sin\phi \sin\theta & 0 \end{bmatrix}, \tag{21}$$

and the antenna response to the polarization is

$$\Delta\xi = \tfrac{1}{2} h_{\alpha\beta} A^{\alpha\beta} = \tfrac{1}{2} h_s s_{\alpha\beta} A^{\alpha\beta} = -h_s l \cos\theta \sin 2\phi \ . \tag{22}$$

The antenna response patterns in the polar and azimuthal directions are shown in Fig. 5.

When we analyze the response of each arm individually we see that each has a $\cos^2\theta$ radiation pattern, similar to that of a simple mass quadrupole, and is the same as that of an elastic solid bar antenna (neglecting Poisson ratio effects). The combined antenna pattern is thus seen to be the coherent addition of two orthogonal $\cos^2\theta$ type patterns.

The total combined response of the antenna to the radiation of arbitrary polarization is a complex shape—an artist's conception of the pattern is shown in Fig. 6.

When the antenna was operated as a detector for gravitational radiation, it was situated in the basement laboratory of the Hughes Research Laboratories, Malibu, California. The Research Laboratories are located at 119° west longitude and 34° north latitude. The arms of the antenna were tangent to the earth's surface and were pointing at 53° and 143° from north.

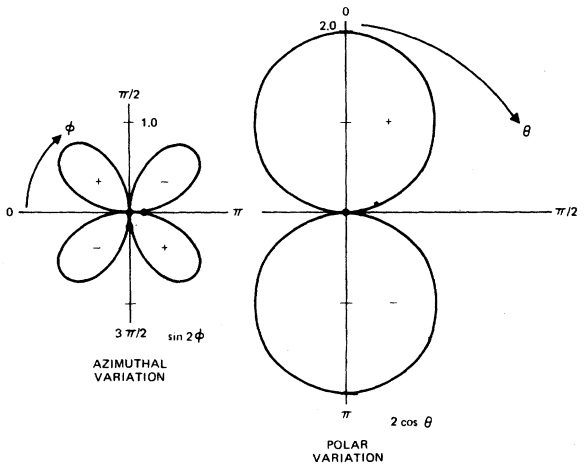

FIG. 5. Detection sensitivity pattern for linearly polarized gravitational radiation with a bisector of the polarization directions in the plane of the antenna.

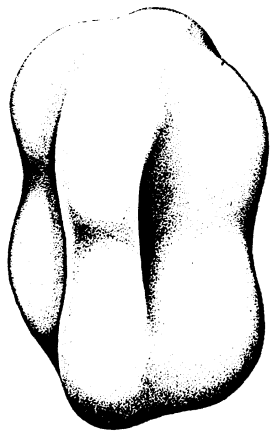

FIG. 6. Radiation pattern of Malibu wideband-interferometric gravitational antenna.

From Fig. 6 we see that the major response of the antenna was in the directions normal to the plane of the antenna. The secondary-response characteristics of the antenna were along the four tangential lobes aligned with the antenna arms. If we translate the antenna pattern to the center of the earth, then the main lobes were at

119° west longitude, 34° north latitude—Malibu,
61° east longitude, 34° south latitude—Southwest Pacific,

while the four tangent lobes lie on a great circle with Malibu as the center and were located at

7° west longitude, 29° north latitude—Morocco,
173° east longitude, 29° south lattitude—New Zealand,
65° west longitude, 43° south latitude—Argentina,
115° east longitude, 43° north latitude—Gobi Desert.

(One pair of antenna nulls was oriented close to the polar directions.)

The New Zealand lobe strongly overlaps the antenna patterns of the Glasgow bar antennas, while the Argentina and Gobi Desert lobes overlap the Maryland bar-antenna pattern.

For the night hours of the fall of 1972, the center of the galaxy passed under the earth so the antenna sensitivity was a maximum for gravitational radiation from that direction. With the combination of the multilobed pattern and the earth rotation, most of the sky (except for the poles) was scanned during the period data was collected.

II. ANTENNA DESIGN

A. Interferometer

The interferometer used was a folded Michelson interferometer. The light source for the interferometer was a large laser on a 3-m granite slab

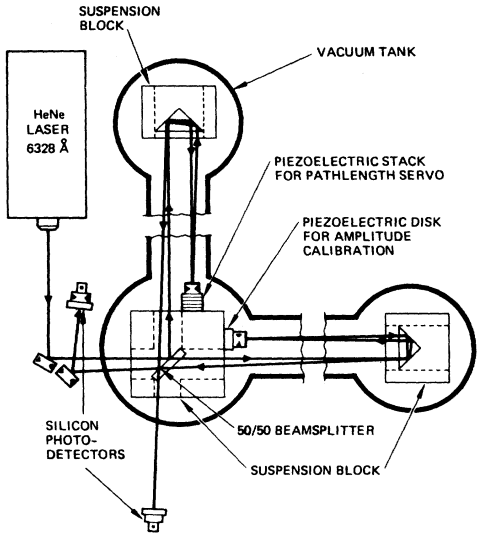

FIG. 7. Schematic of folded optical path.

on low-frequency air mounts. As is shown in Fig 7, the beam from the laser enters through a window in a 0.5-m-diameter cylindrical vacuum tank and is separated into two beams by a 50/50 beamsplitter inside. One beam travels down a 2 m length of evacuated aluminum irrigation pipe to a second cylindrical vacuum tank containing a high-quality optical-corner-cube retroreflector. The beamsplitter and retroreflectors were mounted in support blocks designed to have no internal mechanical resonances below 25 kHz. The reflected beam returns down the pipe to the center vacuum tank where it strikes a mirror mounted on the same support block as the beamsplitter. The mirror is also coupled to a stack of piezoelectric length transducers that are used in a low-frequency servo system to maintain the interferometer pathlength constant at the lower frequencies. The beam returns to the retroreflector where it is again reflected (in the process canceling some of the optical errors in the retroreflector) and sent back down to the beamsplitter.

The second beam from the beamsplitter travels down another evacuated section of pipe to another cylindrical vacuum tank mounted on a separate vibration isolation table. The laser beam in this arm is reflected from the retroreflector and returns to a mirror also mounted on the same block as the beamsplitter. This mirror is coupled to a piezoelectric disk that can be driven with calibrated voltages to induce a known high-frequency mirror motion that can be used to calibrate the interferometer. This beam also goes back through its retroreflector and returns to the beamsplitter where it is combined with the first beam. In this folded configuration, the effective length of each arm is 4.25 m. For gravitational radiation orthogonal to the plane of the interferometer, the effective length of the interferometer is 8.5 m.

The combined beams from the two arms were then brought out through windows where they were detected by a differential pair of silicon photodetectors.

B. Isolation system

The primary isolation table for the interferometer was a $0.3 \times 1 \times 3$ m 2300-kg granite slab on four Firestone 1×84D-1 air mounts. The resulting combination had a resonant frequency of approximately 1.5 Hz.

A second isolation table of $0.3 \times 1 \times 1$ m granite slab on similar air mounts was used for support of the other arm of the interferometer. The interferometer was enclosed in a vacuum housing that was kept evacuated to nominal forepump vacuum levels (< 100 μ Hg).

The vacuum system and isolation tables were designed so that after an initial checkout and operation with 2-m sections of aluminum irrigation pipe (8.5 m total interferometer pathlength), those sections could be replaced with longer sections (up to 1 km) with a substantial increase in interferometer-gravitational radiation-strain sensitivity for the same photon-noise-limited displacement sensitivity.

C. Retroreflectors

The retroreflectors used at the ends of the arms in the interferometer were 5-cm-diameter fused-silica corner cubes. The return beam from a corner retroreflector is elliptically polarized. If, however, the beam is reflected back on itself, then the ellipticity of the polarization is corrected. This characteristic of the retroreflector and the desire to have all the active components in the system at one location (near the beamsplitter), to keep the remote portions of the antenna as simple as possible, led to the folded-beam configuration of Fig. 7. A flat mirror was used for the intermediate reflection at the end of the beam (back at the beamsplitter) to prevent beam translation with corner rotation.

D. Suspensions

The beamsplitter and the retroreflectors were mounted in holes bored into aluminum cubes approximately 10 cm on a side. With these dimensions, the first longitudinal vibrational mode is about 25 kHz, above the 1 to 20 kHz search band. No additional modes in the 1 to 20 kHz band should have been generated by the holes. These optical support blocks were placed on top of stacks of alternating 6-mm neoprene rubber pads and 2.5-

cm brass plates stacked to the desired height. These suspensions had a typical frequency of 10 Hz. Although they would not be adequate in a search for radiation at pulsar frequencies 0.1 → 100 Hz, they were more than adequate for a search in the 1 to 20 kHz band.

E. Laser

The laser used in the interferometer was a modified Spectra-Physics Model 125, which nominally emits a 65-mW multimode. The laser was first modified by a new etalon design[6] to produce between 35 to 55 mW single mode. The new etalon design had high stability (11 min. between mode hops) and low noise, except when the etalon was exactly on its center mode, when it was noticeably noiser.

The noise in the 1 to 20 kHz region was further reduced by replacing the Spectra-Physics power supply with a Fluke precision high-voltage power supply, and then deliberately inducing a laser-plasma oscillation at 100 kHz. With these modifications, the laser noise was drastically reduced from the normal noise level of the Model 125. Figure 8 shows the laser-noise spectrum for 9 mA of detector current as measured through a 10-Hz bandwidth filter. The actual laser noise above 2 kHz is about 5 times the photon-noise limit of the detected photons.

The noise measurement was then repeated using a beamsplitter and optics to simulate the balanced detector operation of the actual interferometer. Figure 9 shows the laser-noise spectrum as measured by a pair of balanced photodetectors, each carrying about 2.2 mA of photoelectrons. The measured noise is now very close to the photon-noise limit of the detected photons.

F. Photodetection system

The photodetectors used in the interferometer were United Detector Technology Type PIN-25 Schottky barrier photodiodes. They had an active area of 6 cm^2 (2.8 cm diameter) and a linear range of 10 mW/cm^2 (better than 60 mW per detector). This was more than adequate for the 10 to 20 mW expected at each detector. The linearity of the detectors used in the interferometer was checked up to 6 mA of detected current (about 24 mW incident power).

The optical transmission through the interferometer beamsplitter mirrors and retroreflectors was measured as 0.7. The reflection loss at each photodetector was 0.6 and the quantum detection efficiency was 0.7, for a combined optical efficiency of 0.3. Thus, for a nominal 35 mW of single-mode laser power, 24 mW made it through

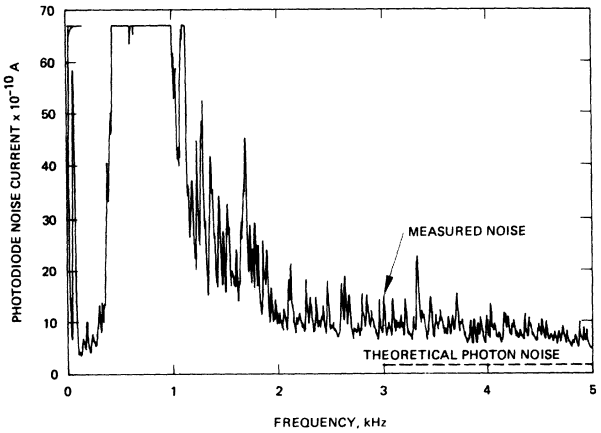

FIG. 8. Laser noise measured in 10-Hz bandwidth.

the interferometer, 14 mW reached the photodetector, and 10 mW was detected. All of these efficiencies could have been improved somewhat with further effort. The most obvious improvement would have been to have the photodetectors fabricated with a front surface-contact layer that would be compatible with an antireflection coating.

The photodiodes were operated at a nominal bias voltage of 10 V, which gave a capacitance of 1700 pF and a dark current of 5 μA. The load resistor used with the photodiodes was nominally 5 kΩ which gave a 3 dB frequency rolloff at 20 kHz.

The photodetectors were operated as a balanced pair in a circuit configuration (see Fig. 10) with a special filter that allowed the signals in the 0.5 to 25 kHz band to pass on to the preamplifier while blocking the high-frequency plasma oscillation at 100 kHz (induced for laser-noise reduction) and the low-frequency line harmonics that could have saturated the preamplifier.

The circuit also allowed for the extraction of the

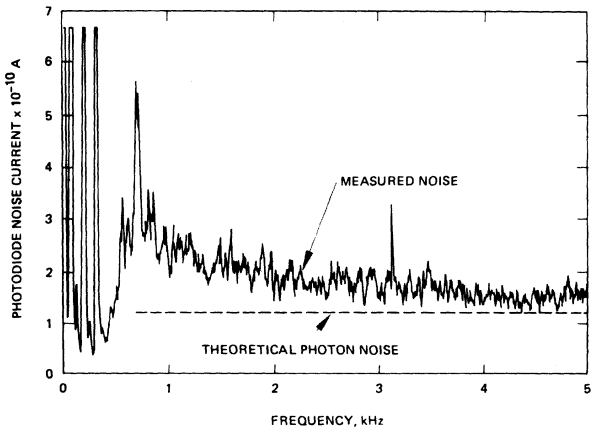

FIG. 9. Laser noise in 10-Hz bandwidth with balanced detectors.

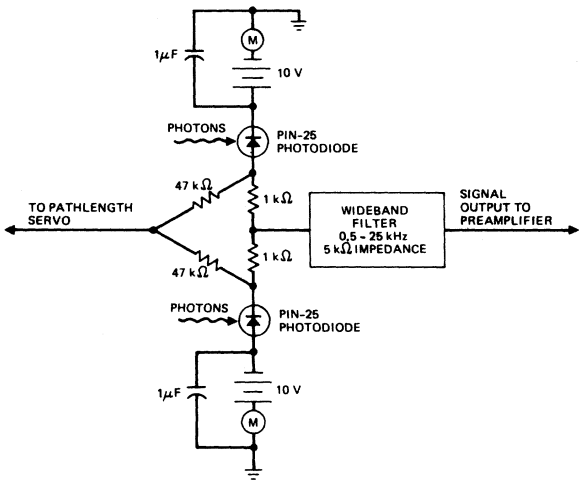

FIG. 10. Photodiode bias and filter circuit.

160-Hz pathlength servo signal that was used in a narrow-band feedback circuit to control a piezoelectric stack in one arm of the interferometer to maintain equal illumination of the two photodetectors.

The bandpass filter used in the circuit was a special design consisting of a 5 kΩ impedance, 5-pole, high-pass Butterworth filter with a low-frequency rolloff of 550 Hz and a slope of 26 dB/octave. This was followed by a 5 kΩ impedance, 5-pole, low-pass, Tschebyscheff filter with a high-frequency rolloff of 25 kHz and a slope of 30 dB/octave (see Fig. 11) The insertion loss of the filter was less than 1 dB from 1 to 20 kHz (see Fig. 12).

III. INTERFEROMETER *S/N* ANALYSIS

In the Michelson interferometer shown in Fig. 13, the single-mode laser power P entering the interferometer produces a photon flux at the entrance to the beamsplitter of

$$\phi_0 = \frac{P}{h\nu} \ , \tag{23}$$

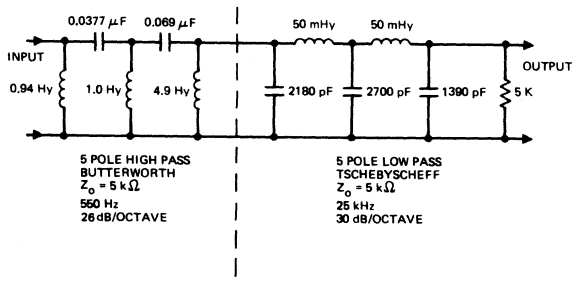

FIG. 11. Low-insertion loss wideband filter.

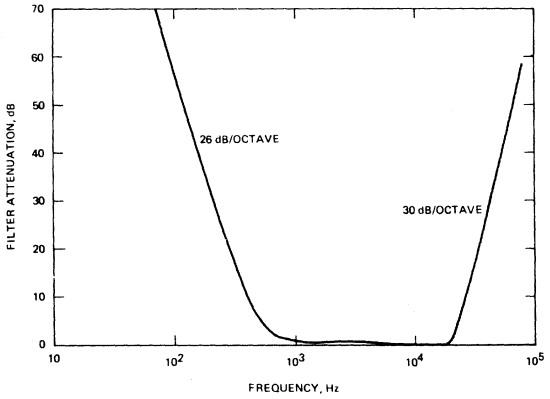

FIG. 12. Filter bandpass attenuation.

where

$$h = 6.626 \times 10^{-34} \text{ J sec} \ ,$$

$$\nu = 4.74 \times 10^{14} \text{ Hz} \ ,$$

$$h\nu = 3.14 \times 10^{-19} \text{ J} \ .$$

(A single-mode laser power of 50 mW is equivalent to a photon flux of 1.6×10^{17} photons/sec.)

The laser beam is divided at the 50-50 beamsplitter. One half travels down arm one and is delayed by the pathlength $\zeta_1 = l_1 + \xi_1(t)$ of arm one, while the other half travels down arm two and is delayed by that pathlength $\zeta_2 = l_2 + \xi_2(t)$. On their return to the beamsplitter, the two beams are again split and one half of each beam is combined with one half of the other at the two photodetectors.

The photon flux reaching the two photodetectors is then given by

$$\phi_1 = \eta \frac{\phi_0}{2} \left[1 - \cos \frac{4\pi}{\lambda} (\zeta_1 - \zeta_2) \right], \tag{24}$$

$$\phi_2 = \eta \frac{\phi_0}{2} \left[1 + \cos \frac{4\pi}{\lambda} (\zeta_1 - \zeta_2) \right], \tag{25}$$

where η is the transmission efficiency of the optics

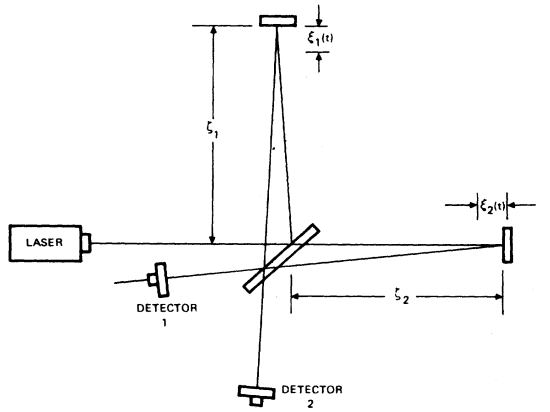

FIG. 13. Michelson interferometer schematic.

in the interferometer, and the difference in the pathlengths of the two arms of the interferometer is

$$\zeta_1 - \zeta_2 = l_1 - l_2 + \xi_1 - \xi_2$$

or

$$\Delta\zeta = \Delta l + \Delta\xi \ . \tag{26}$$

The detectors were operated in a differential signal mode. For maximum sensitivity the nominal pathlength l_1 of one arm was adjusted by the low-frequency pathlength servo so that there was nominally half the total power on each detector. This occurs when

$$\frac{4\pi\Delta l}{\lambda} = \frac{\pi}{2} \pm \pi \tag{27}$$

or

$$\Delta l = \frac{\lambda}{8} \pm \frac{\lambda}{4} \ . \tag{28}$$

At this interferometer setting,

$$\cos\frac{4\pi}{\lambda}(\Delta l + \Delta\xi) = -\sin\frac{4\pi}{\lambda}\Delta\xi \approx -\frac{4\pi}{\lambda}\Delta\xi \tag{29}$$

[where we have assumed $\Delta\xi(t)$ is small compared to the wavelength].

The flux incident at the two detectors is then

$$\phi_1 = \eta\frac{\phi_0}{2}\left(1 + \frac{4\pi}{\lambda}\Delta\xi\right) , \tag{30}$$

$$\phi_2 = \eta\frac{\phi_0}{2}\left(1 - \frac{4\pi}{\lambda}\Delta\xi\right) . \tag{31}$$

As the pathlength difference $\Delta\xi(t)$ due to the gravitational-radiation strains changes with time, the flux at one detector will increase, while the flux in the other will decrease.

In a measurement time interval τ, the number of photoelectrons produced in each detector is

$$N_1 = \frac{\eta\phi_0\tau}{2}\left(1 + \frac{4\pi}{\lambda}\Delta\xi\right) , \tag{32}$$

$$N_2 = \frac{\eta\phi_0\tau}{2}\left(1 - \frac{4\pi}{\lambda}\Delta\xi\right) , \tag{33}$$

where the quantum efficiency of the photodetector is now included in the efficiency coefficient η.

The number of photoelectrons in each photodetector has an average value[7] of

$$\langle N_1\rangle = \langle N_2\rangle = = \tfrac{1}{2}(\eta\tau\langle\phi_0\rangle) , \tag{34}$$

and a variance of

$$\mathrm{var}N_2 = \mathrm{var}N_1 = \langle(N_1 - \langle N_1\rangle)^2\rangle = \langle N_1\rangle \tag{35}$$

that is proportional to the average number of detected photons.

Each measurement interval has a measured number of photoelectrons that is different (usually) from the average number; this difference,

$$\Delta N_1 = N_1 - \langle N_1\rangle \ , \tag{36}$$

is greater or less depending upon the length of the measurement time (number of measured photoelectrons). The time average of this difference is

$$\Delta n_1 = \frac{\Delta N_1}{\tau} \ . \tag{37}$$

The spectral intensity in photoelectrons^2/sec^2 Hz of the noise is then given by[7]

$$\begin{aligned} S(f) &= \lim_{\tau\to\infty} 2\tau\langle\Delta n_1^2\rangle \\ &= \lim_{\tau\to\infty} 2\frac{\langle\Delta N_1^2\rangle}{\tau} \\ &= \lim_{\tau\to\infty} \frac{2\langle N_1\rangle}{\tau} \\ &= \eta\langle\phi_0\rangle \\ &= \frac{\eta\langle P\rangle}{h\nu} \ . \end{aligned} \tag{38}$$

This spectral intensity of photoelectron noise S produces a squared noise current in a bandwidth B given by

$$\begin{aligned} I_{n_1}^2 = I_{n_2}^2 &= e^2SB \\ &= e^2\eta\langle\phi_0\rangle B = \frac{\eta\langle P\rangle e^2B}{h\nu} \\ &= 2e\langle I\rangle B \ , \end{aligned} \tag{39}$$

where $\langle I\rangle = \frac{1}{2}(\eta\langle\phi_0\rangle)e$ is the average photocurrent in each photodetector. The noise current is the same in both photodetectors since their average detected flux levels are kept equal.

The signal currents and the noise currents from the photodetectors are converted into voltages by means of the load resistor of nominal resistance $R \approx 5$ kΩ that terminates the wideband filter (see Fig. 11). The load resistor also contributes the following Johnson noise voltage:

$$\begin{aligned} &V_R^2 = 4kTBR \ , \\ &\text{where} \\ &k = 1.38\times10^{-23}\ \text{J/K} \ , \\ &T = 290\ \text{K} \ . \end{aligned} \tag{40}$$

The Johnson noise of a 5-kΩ resistor in a 10-Hz bandwidth is

$$\begin{aligned} V_R &= (4kTBR)^{1/2} \\ &= 27\ \text{nV} \ . \end{aligned} \tag{41}$$

During the operation of the interferometer, the

load resistor was carrying a photocurrent that was never less than 2 mA. This level of photocurrent would generate in a bandwidth of 10 Hz, a noise voltage due to shot noise of the photoelectrons of

$$V_P = (2eIB)^{1/2}R = 370 \text{ nV} . \quad (42)$$

Thus, in all cases, the photocurrent shot noise was very much larger than the Johnson noise in the load resistor, so we can ignore the noise contribution of the Johnson noise in our analyses.

The low-noise differential amplifier used in the experiment was a PAR CR-4, with selected front-end FETs. The amplifier noise figure for the 5-kΩ load was 0.2 dB. This had a negligible effect on the overall system performance.

The time-varying signal voltages are coherent, while the photoelectron noise currents are incoherent. Thus the differential amplifier measures a squared signal voltage as follows:

$$V_S^2 = (V_1 - V_2)^2 = (I_1 - I_2)^2R^2 = (\phi_1 - \phi_2)^2e^2R^2 = \left(\frac{\eta\phi_0 4\pi\Delta\xi}{\lambda}\right)^2 e^2R^2 , \quad (43)$$

while in a bandwidth B it measures a squared shot-noise voltage given by

$$V_n^2 = V_{n_1}^2 + V_{n_2}^2 = (I_{n_1}^2 + I_{n_2}^2)R^2 = 2e^2\eta\phi_0 BR^2 . \quad (44)$$

Thus the signal-to-noise (S/N) power of the measured differential signal is

$$\frac{S}{N} = \frac{2\eta\phi_0}{B}\left(\frac{\Delta\xi}{\lambda}\right)^2 . \quad (45)$$

For unity S/N, the detection sensitivity is then

$$\frac{\Delta\xi^2}{B} = \frac{\lambda^2}{2\eta\phi_0} = \frac{\lambda^2}{2\eta P/h\nu} = \frac{\lambda^2}{2I/e} , \quad (46)$$

where ϕ_0 and P are the initial flux and power of the laser, η is the light incident to photoelectron-conversion efficiency, and I is the combined photocurrent of the two detectors.

For $\eta P = 10$ mW of detected laser power, the theoretical photon-noise limited displacement sensitivity is

$$\frac{\Delta\xi}{B^{1/2}} = \frac{\lambda}{(2\eta P/h\nu)^{1/2}} = 0.4 \text{ fm/Hz}^{1/2} . \quad (47)$$

If we assume an interferometer pathlength of 8.5 m, this converts to a strain sensitivity of 0.5×10^{-16} m/m Hz$^{1/2}$.

IV. DISPLACEMENT TRANSDUCER CALIBRATION

To calibrate the interferometer for displacement sensitivity we used a piezoelectric disk attached to the back of one of the interferometer mirrors (see Fig. 7). The mirror was first driven by a high dc voltage on the piezoelectric until the illumination on the photodetectors went from minimum to maximum. The interferometer pathlength thus had changed by $\lambda/2$ and the mirror had moved $\lambda/4$. The displacement sensitivity obtained was

$$\sigma = 1.6 \times 10^{-10} \text{ m/V} . \quad (48)$$

The drive on the piezoelectric crystal was then reduced from a very high level down to a drive level where the signal was hidden by the laser noise. During this decrease in the drive level the interferometer output remained a linear function of the drive level (to within the noise level of the measurements).

The piezoelectric displacement calibration technique was also cross-checked at the low drive levels by the use of a potassium dihydrogen phosphate (KDP) optical modulator. The KDP modulator was calibrated for a half-wavelength path difference and found to have a displacement sensitivity of

$$\sigma_k = 2.0 \times 10^{-11} \text{ m/V} . \quad (49)$$

The voltage on the KDP pathlength modulator was then reduced to where it gave the same interferometer response as the piezoelectric displacement transducer. The calculated pathlength difference from the KDP modulator was 1.0 pm, within 10% of the displacement calculated for the piezoelectric modulator for the same interferometer output.

V. INTERFEROMETER SENSITIVITY

The sensitivity of the interferometer as a function of frequency was determined by a frequency scan of the interferometer output using a spectrum analyzer with a 10-Hz bandwidth filter (see Fig. 14). During the scan a calibration signal of 100 μV rms was placed on the calibration piezoelectric displacement transducer to insert a 16-fm amplitude signal. The amplitude of the calibration signal was about 5.7 times the noise level in the region between 4 and 5 kHz. The amplitude of the noise measured through a 10-Hz bandwidth filter in that region is therefore about 2.8 fm or 0.9 fm for a 1-Hz bandwidth.

If we assume that the effective length of the interferometer is 8.5 m then the equivalent strain sensitivity is 0.1 fm/m per root Hz at the higher frequencies, rising slightly to 0.3 fm/m per root Hz at 1 kHz. For comparison, the kT strain noise

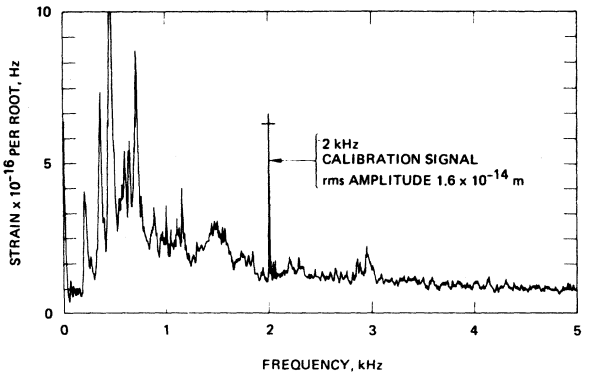

FIG. 14. Strain sensitivity of interferometer antenna.

in a room-temperature, 2-m long, 1000-kg elastic solid bar antenna is 0.14 fm/m.

VI. OPERATION OF THE ANTENNA

Our ultimate plan for the antenna system was to move the interferometer to a remote site and replace the 2-m evacuated pipes with much longer sections of evacuated irrigation pipe. Similar laser interferometer systems up to a kilometer in arm length had already been demonstrated by many others for geophysical studies.[8] Since the sensitivity of the interferometer was fixed at a certain level of displacement sensitivity by the photon noise, an increase in interferometer arm length should give a proportional increase in strain sensitivity for the same laser-power level. The funding for this next move proved to be unavailable so we concluded the program by operating the system as it was, despite the high level of acoustic, electromagnetic and vibrational noise from the other activities in the building.

Since the output of the laser interferometer was a wideband analog signal in the audio region, the signal was recorded directly onto magnetic tape through one channel of a high quality stereo tape recorder. The other channel of the recorder was used as the monitor channel. To monitor the system and environmental noises we combined the outputs of a photodetector to detect the audio-frequency noises in a sample of the laser beam, a microphone to detect acoustic noises in the room, a wideband seismometer to detect floor motion, and an amplifier to detect audio voltages on the power lines. The combined signal was then placed on the monitor channel.

To provide a constant time and amplitude calibration, an accurate 2-kHz signal of about 10-fm amplitude was maintained on the calibration transducer. At 15-min intervals, the time from WWV would be acoustically introduced into the system and recorded on both channels.

Later analysis of the magnetic tapes revealed that about once every two minutes there would be a short coherent signal audible to the ear over the white-noise hiss of the photon noise. Most of these were chirps from a spurious laser mode mixing with the main laser mode, clicks as the laser switched modes, and tones from thermal contractions exciting mechanical vibrations in structures. Nearly all of these were also found in the monitor channel. About once every ten minutes there would be an audible chirp or tone that was not on the monitor channel. Some of these were digitally analyzed and compared with the calibration signal. A typical audible signal was about 1 to 5 times the power of the calibration signal or about 20 to 100 times the photon-noise limit in a 1-Hz bandwidth.

VII. CALIBRATION OF EAR

When the interferometer was working well, we were able to hear single-frequency 3- to 10-kHz tones of 10-fm rms amplitude introduced into the interferometer by the piezoelectric displacement transducer.

Since the noise level of the interferometer in that band is about 0.9 fm/$Hz^{1/2}$, this means that the audio system, including our ear-brain combination, had an effective detection bandwidth of about 120 Hz.

Although the detection capability for single tones, chirps, and impulsive events will be different, we feel that if we were listening carefully for a signal that exceeded an rms amplitude of about 10 fm or a strain amplitude of 1 fm/m, that we would have detected it by ear. We could then pin down the exact position on the tape and carry out a detailed digital analysis of that section of tape that would produce data with time resolution of 40 μsec, amplitude resolution of 0.9 fm/$Hz,^{1/2}$ and strain resolution of 0.1 fm/m $Hz^{1/2}$.

However, because of the uncertainties in the signatures of gravitational-radiation signals and the capability of our ear-brain combination to recognize an unknown signature as something "unusual" in a background of white noise, we will be conservative and say only that a gravitational wave with a total strain level of 10 fm/m over the audio band (1 to 20 kHz), would have been easily detected by ear on our tapes.

To give an example of the detailed structure that can be extracted from a short signal with a sophisticated digital signal processor replacing the analog ear-brain signal processing system, we analyzed one short (~10 msec) tone that occurred at 09 h 46 min 21 sec GMT Sunday 3 December

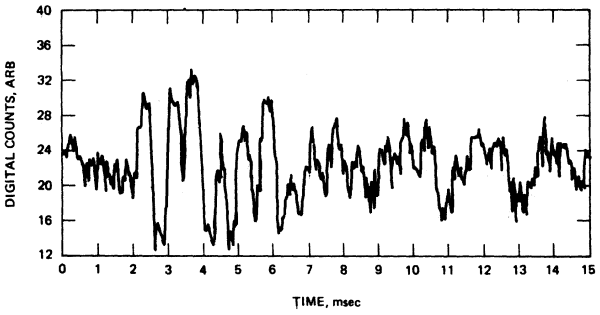

FIG. 15. Time history of typical signal.

1972. The detailed signature can be seen in the digitized time history of the signal (see Fig. 15), and the frequency spectrum can be seen in the power spectral density plot of Fig. 16. (The peak at 3000 Hz is the calibration signal of about 10 fm.) Although this signal occurred within 3 sec. of a coincidence between the two 1660 Hz antennas in the Maryland system, it is not a good candidate. The energy at 1660 Hz is negligible and the time delay exceeds the estimated errors in the measurement of absolute time (0.6 sec) in the two systems.

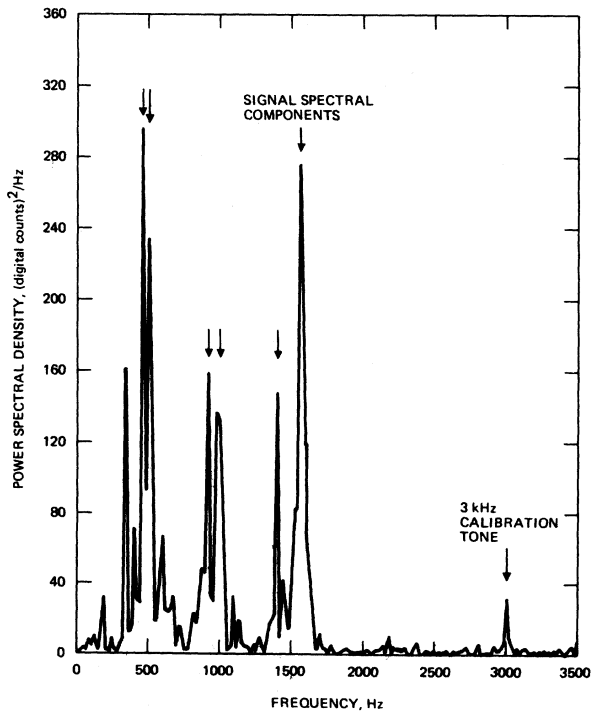

FIG. 16. Power spectral density plot of typical signal.

VIII. COMPARISON OF DATA WITH OTHER OBSERVERS

During October 1972 the Frascati group were operating a single elastic-solid type gravitational-radiation antenna.[9] During the hours when the Malibu antenna was in operation between the dates from 15 to 25 October 1972, the Frascati group recorded 18 instances when the antenna output produced a significant level of response. None of these coincided with a signal in the Malibu antenna.

During the fall of 1972, the Glasgow group were operating a pair of wideband (BW $\approx$ 800 Hz) elastic-solid type antennas. During the hours when the Malibu antenna was in operation, their system responded to 22 events where the signal from one or the other of their two antennas exceeded a previously set threshold. None of these coincide with a signal in the Malibu antenna. The one "distinctive signal" reported by the Glasgow group[10] occurred at 13 h 07 min 29 sec GMT 5 September 1972, which was prior to the start of the Malibu data collection period.

Gravitational-radiation antennas of the elastic-solid type have been under development at the University of Maryland since 1959.[11] Statistically significant numbers of coincidences between antennas at the University of Maryland and the Argonne National Laboratory have been reported since 1969.[12]

During the fall of 1972, the Maryland group was recording coincidences between a 66-cm diameter, 1.5-m long resonant aluminum cylinder at College Park, Maryland and a similar cylinder at Argonne, as well as coincidences between a resonant aluminum disk at College Park and the cylinder at Argonne. The Argonne and College Park cylinders had a nominal resonant frequency of 1660 Hz. The disk was originally designed to search for 1660-Hz scalar radiation and was constructed to have a radially symmetric mode at 1660 Hz that would be excited by scalar radiation. It was also instrumented to detect a mode at 1100 Hz that would only be excited by tensor gravitational radiation.

During the time that the Malibu antenna was operational, the Maryland group recorded 28 coincidences between either the bar at Argonne and the bar at Maryland, or the bar at Argonne and the disk at Maryland. Because of triple coincidences and close-spaced coincidences, the 28 Maryland coincidences fell into 20 two-minute time blocks. Of the 20 time blocks, 7 blocks (containing 17 coincidences) had audible signals in the Malibu interferometer that were within 10 sec of the Maryland coincidences and were not audible in the monitoring channel.

Both raw power and derivative power-squared digitized data plots digitized to 0.1-sec accuracy were obtained from the Maryland group and compared with the 0.2-sec accuracy Malibu data. None of the audible Malibu signals fell within 0.6 sec of a Maryland-Argonne coincidence.

It is difficult to compare the relative detection capabilities of the various antennas since their amplitude sensitivities, bandwidths, and signal processing techniques differ widely.

In general we can say that the bar-antenna detection systems responded to gravitational-radiation strains with spectral components near the resonant frequency of the bar that had an amplitude of the order of 0.1 fm/m, while the interferometer antenna responded to gravitational-radiation strains with spectral components in the band from 1–20 kHz. The sensitivity of the interferometer is highly dependent upon the signature of the signal and the processing technique and varies from 0.1 fm/m for known narrow-band signals to 10 fm/m for noiselike signals.

However, the lack of a significant correlation between the interferometer output and the bar events and coincidences can be used to put an upper limit on the gravitational-radiation strain amplitude during the bar coincidences and events. Thus, at the time one of the bar-antenna systems produced an event or coincidence corresponding to a gravitational-radiation signal with an amplitude of 0.1 fm/m due to spectral components in a narrow band around the bar resonance, the amplitude of the gravitational-radiation spectral components in the entire band from 1–20 kHz was definitely less than 10 fm/m and was probably less than 1 fm/m.

ACKNOWLEDGMENTS

The work on the design, construction, operation, and data analysis of the wideband laser-interferometer antenna was a multiyear effort involving many people.

The initial design and studies were carried out by Gaylord Moss, Larry Miller, and Jay Melosh, with advice from Philip Chapman and Ranier Weiss. The construction of the steadily more complex and capable designs were predominantly the brilliant work of Gaylord Moss with some inspired early feasibility demonstrations by Larry Miller. Mr. Moss and Mr. Miller were ably assisted by Larry Matheney, Don Boswell, Ken Craig, Cesar DeAnda, Ismael Charnabroda, Craig Spencer, and Dale Sipma at various times during the program. The operation of the laser interferometer as a detector for gravitational radiation required a dedicated effort which involved sitting nearly motionless for hours at a time, monitoring the interferometer and data collection system performance. I was ably assisted on alternate shifts by Gaylord Moss, who often collected data all night and spent the next day fixing a balky laser or piece of electronics.

The data analysis was another long and arduous effort which was made much easier by the able assistance of Ray Lahr in the double-blind audio analysis and the Hughes digitalization and display facility operated by Brad Tuttle and Al Rieser.

I would also like to acknowledge the encouragement, cooperation, and exchange of data of the other groups who were operating gravitational-radiation detectors at the same time—Professor R. W. P. Drever and Roger Bland of the University of Glasgow, Dr. K. Maischberger of the European Space Research Organization, Frascati, Italy and especially Professor J. Weber and Bruce Webster of the University of Maryland.

I finally would like to thank Dr. George Smith and the Hughes Aircraft Company for the moral and financial support during the three years it took to get the system operational.

[1]G. E. Moss, L. R. Miller, and R. L. Forward, Appl. Opt. 10, 2495 (1971).
[2]R. L. Forward and G. E. Moss, American Physical Society Winter Meeting, Los Angeles, CA, 1972 (unpublished).
[3]R. L. Forward, Gen. Relativ. Gravit. 2, 149 (1971).
[4]L. Landau and E. Lifshitz, *The Classical Theory of Fields* (Addison-Wesley, Reading, Mass., 1951), p. 326.
[5]H. Goldstein, *Classical Mechanics* (Addison-Wesley, Cambridge, Mass., 1956), pp. 107–109.
[6]G. E. Moss, Appl. Opt. 10, 2565 (1971).
[7]A. van der Ziel, *Noise* (Prentice Hall, Englewood Cliffs, New Jersey, 1971), pp. 14–16.
[8]V. Vali and R. C. Bostrom, Earth Planet. Sci. Lett. 4, 436 (1968).
[9]D. Bramanti and K. Maischberger, Lett. Nuovo Cimento 4, 1007 (1972).
[10]R. W. P. Drever *et al.*, Nature 246, 340 (1973).
[11]J. Weber, Phys. Rev. 117, 306 (1960).
[12]J. Weber, Phys. Rev. Lett. 22, 1320 (1969).